Erschienen in: Materials Today ; 10 (2007), 5. - S. 40-48

ZnO – nanostructures, defects, and devices

ZnO has received much attention over the past few years because it has a wide range of properties that depend on doping, including a range of conductivity from metallic to insulating (including *n*-type and *p*-type conductivity), high transparency, piezoelectricity, wide-bandgap semiconductivity, room-temperature ferromagnetism, and huge magneto-optic and chemical-sensing effects. Without much effort, it can be grown in many different nanoscale forms, thus allowing various novel devices to be achieved. We review recent studies of ZnO nanostructures, fabrication, novel device applications, and its potential as an electron-acceptor material in hybrid solar cells. Control of its rich defect chemistry, which is critical for controlling properties but has not been widely addressed in the context of novel applications, is also discussed.

Lukas Schmidt-Mende* and Judith L. MacManus-Driscoll
Department of Materials Science, University of Cambridge, Pembroke Street, CB2 3QZ, Cambridge, UK
**E-mail: ljs38@cam.ac.uk*

The interest in ZnO structures has increased drastically in recent years. Intense research by many different groups has focused on novel nanostructures with different shapes ranging from nanowires to nanobelts and even nanosprings. The number of reviews on ZnO is increasing (see for example[1-9]). The topic of *p*-doping is especially difficult and has been investigated by different groups[10-13]. ZnO is a direct wide bandgap (~3.3 eV)[2] material with a large exciton binding energy of 60 meV. This makes it interesting as a laser material based on exciton recombination at room temperature or even higher.

Such a large amount of research on ZnO nanomaterials makes it hard to summarize the work in a systematic way. In this article, we first describe different synthesis routes toward a large variety of nanostructures. The first approach is chemical vapor deposition; certainly one of the most common routes for the synthesis of nanowires, nanobelts, nanosprings, and nanorings. Aqueous solution growth has also attracted great interest. This method allows growth of nanowires and other nanostructures at low temperatures. We describe this method in some detail. Similar to aqueous solution growth, electrodeposition of ZnO nanocolumns can be performed at low temperatures, and this is also briefly described.

A very important issue is the doping of ZnO nanowires. We give an introduction into the defect states of ZnO and describe different examples where doping of ZnO nanowires and thin films has been performed. The last section focuses on applications of ZnO nanowires. We describe their use as sensors and cantilevers, as well as their

ISSN:1369 7021 © Elsevier Ltd 2007

application in optoelectronic devices, such as light-emitting diodes and solar cells.

Synthesis of ZnO nanostructures

ZnO has probably the richest variety of different nanostructures. Its range includes highly ordered nanowire arrays, tower-like structures, nanorods, nanobelts, nanosprings, nanocombs, and nanorings. We address the synthesis routes for a number of these structures. The literature on ZnO nanostructures is immense and we can only describe a small selection of work. We start with structures that can be obtained using chemical vapor deposition (CVD) and metal-organic CVD, including growth with and without a catalyst.

Chemical vapor deposition

Nanowires and nanorods

In CVD, a vapor reacts on the substrate to produce the desired product. In the case of nanowires, the vapor-liquid-solid (VLS) method usually applies, where the vapor is exposed to a catalyst such as Au particles. This seed layer is enriched by the vapor source material until it is saturated and the desired material starts to solidify and grow outward from the catalyst[14]. Large-scale arrays with vertically aligned nanowires have been produced by this method[15-17]. The partial oxygen pressure and chamber pressure are important parameters influencing the growth mechanism that governs the final structure of the ZnO[18,19]. By increasing the oxygen content under otherwise identical conditions, nanowires, dendritic side-branched/comb-like structures, and nanosheets can be synthesized[20].

The catalyst seed layer has an immense influence on nanowires. Control over nanowire growth can be gained by simply varying the Au layer thickness[21]. Catalytic Au patterns formed by lithography techniques can be used for directed ZnO nanowire growth[22]. This opens the possibility of investigating how light interaction between neighboring nanowires affects collective properties.

Other groups have reported a vapor-solid (VS) process[23]. Epitaxial growth of highly aligned and nearly defect-free nanorods has been observed using CVD (1:1 ZnO:graphite) on an initial ZnO film produced by pulsed laser deposition (PLD)[24]. ZnO nanorods grow on (100) sapphire at a 30° angle to the substrate normal, indicative of epitaxial crystalline growth[25]. The growth of nanocolumns on alumina substrates via oxidation of ZnS in a tube furnace at 950°C has also been reported. The substrates are kept apart from the source at a lower temperature. The synthesized nanocolumns show a layered structure and become gradually thinner. This is assumed to be a result of a gradually decreasing supply of ZnO vapor[26].

Other nanostructures

Nanocombs have been synthesized by thermal evaporation of ZnO powder in a tube furnace (Fig. 1). The comb-like structures grow on an alumina substrate placed downstream, and growth is only observed in the region where the temperature ranges from ~1050-1250°C,

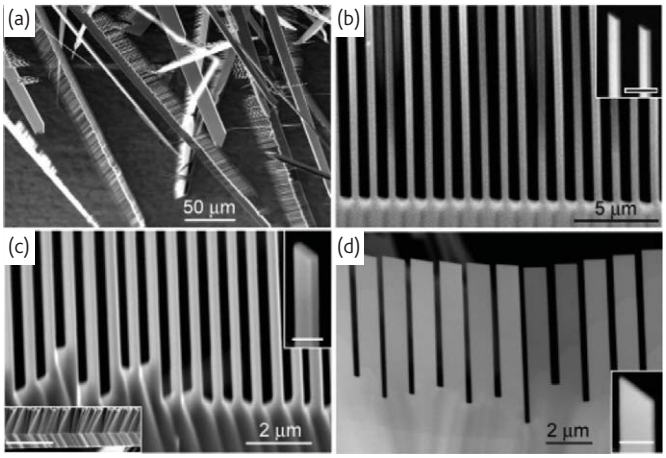

Fig. 1 Scanning electron microscopy (SEM) images of ZnO combs formed by evaporating ZnO powder at 1400°C for 2 hours. (a) Low-magnification SEM image of ZnO combs. (b) High-magnification SEM image of a comb made of an array of rectangular ZnO nanobelts ~400 nm wide at a spacing of ~700 nm. Inset shows the growth fronts of two nanobelts with rectangular cross sections. Scale bar = 1 µm. (c) Array of nanobelts ~280 nm wide at a spacing of ~250 nm. Upper right inset shows the growth front of one rectangular nanobelt. Scale bar = 500 nm. Lower left inset is an SEM image of the stem of a comb. Scale bar = 10 µm. (d) Aligned nanobelts ~500 nm wide at a spacing of ~300 nm. inset is the growth front of a nanobelt. Scale bar = 500 nm. (Reprinted with permission from[27]. © 2005 American Chemical Society.)

regardless of the evaporation temperature. Increasing growth time influences the dimensions of the combs and even the shape of the associated nanowires. These nanocombs with periodical structures could find application as gratings in miniaturized integrated optics[27].

Another catalyst-free synthesis route for large-scale ZnO nanostructures involves heating a Zn foil to 700°C in a furnace in air without any additional carrier gas[28]. By controlling the heating rate, different morphologies have been achieved: porous membranes, nanowires, nanorods, nanoneedles, and nanotetrapods.

Metal-organic CVD

Metal-organic CVD (MOCVD) achieves growth of material via surface reaction of organic or metal-organic precursor compounds containing the required chemical elements. Lee *et al.*[29] have used MOCVD to grow well-aligned, single-crystalline ZnO nanowires on GaAs substrates.

Low-temperature growth routes for ZnO nanorods have also been reported. A two-zone furnace can be used with Zn acetylacetonate hydrate placed as a precursor material into the low-temperature zone of the furnace (130-140°C). The vapor is then carried by 500 sccm N_2/O_2 flow into the higher temperature zone of the furnace with substrates kept at 500°C at 200 torr. The ZnO nanorods grow directly on fused silica or Si substrates[30]. Another low-temperature method uses Zn nitrate hexahydrate and ammonium hydroxide as a precursor. Here, the preparation of the initial ZnO buffer layer significantly affects the morphology and quality of the ZnO nanorods[31]. Air-annealing enhances the crystallinity and optical properties of the nanowires.

Nanobelts and nanorings

By using ZnO powder as a source material without the presence of a catalyst, nanobelts with lengths of several tens to several hundreds of micrometers can be achieved[32]. This growth process is dominated by a vapor-solid process, where the vapor deposits directly onto the substrate, which is held at a lower temperature.

Gao *et al.*[33,34] have reported a method to form nanoribbons that then transform into nanohelices. A horizontal tube furnace with ZnO powder as the source material is used. The solid-vapor deposition is carried out at 1400°C for 2 hours under a pressure of ~200 mbar with Ar as the carrier gas. Nanohelices are deposited onto a polycrystalline Al_2O_3 substrate at a local temperature of 700-800°C. 10% of the synthesized material is composed of freestanding nanohelices, with left- and right-handed chiralities in a 1:1 ratio. The formation of nanorings and nanohelices can be explained using dipole effects. The Zn-terminated <0001> surface is positively charged and the O-terminated <000$\bar{1}$> surface negatively charged. Thus, there is a spontaneous dipole moment along the *c*-axis. For small thicknesses, as found in nanobelts (~10 nm), the spontaneous polarization can produce the structures observed, such as nanorings, nanobows, nanohelices, and nanospirals. This can be explained by the minimization of the energy resulting from polar charges, surface area, and elastic deformation[35,36]. Hughes and Wang[37] have produced nanorings and nanobows by a similar method. ZnO powder is heated to 1350°C for 2 hours in a horizontal tube furnace maintained at a pressure of 300 mbar with an Ar flux of 50 sccm, and the nanorings/bows are collected on an Al_2O_3 substrate at 500°C downstream of the source material. The yield in nanorings is around 5% of the total deposited product. The researchers also observe nanobows and nanobelts bent into semi-rings. Kong *et al.*[38] have used a similar method and observed self-coiling of nanobelts into nanorings. A review article by Wang[39] describes the nanobelt family of metal oxides including ZnO.

Aqueous solution growth

Many groups have reported the growth of highly oriented ZnO nanowires and other nanostructures from aqueous solution. Andrés-Vergés *et al.*[40] reported the aqueous solution growth method for the first time in 1990. More than 10 years later, Vayssieres *et al.*[41] used this method to grow nanorods on conducting glass and Si substrates. For this type of growth, a ZnO seed layer is needed to initialize the uniform growth of oriented nanowires. Often, a solution of $ZnO(NO_3)_2$ and hexamethyltetramine (HMT) is used:

$$(CH_2)_6N_4 + 6H_2O \leftrightarrow 6HCHO + 4NH_3 \quad (1)$$

$$NH_3 + H_2O \leftrightarrow NH_4^+ + OH^- \quad (2)$$

$$2OH^- + Zn^{2+} \rightarrow ZnO(s) + H_2O \quad (3)$$

Hydroxide ions are formed by the decomposition of HMT and they react with the Zn^{2+} to form ZnO.

Fig. 2 shows some typical nanowire arrays grown by our group using this method. For technical applications, it is important to note that this method operates at low temperature and a homogenous coverage of nanowires can be achieved over large areas. (In our work[42], the area is only limited by our substrate size, ~2 cm^2.)

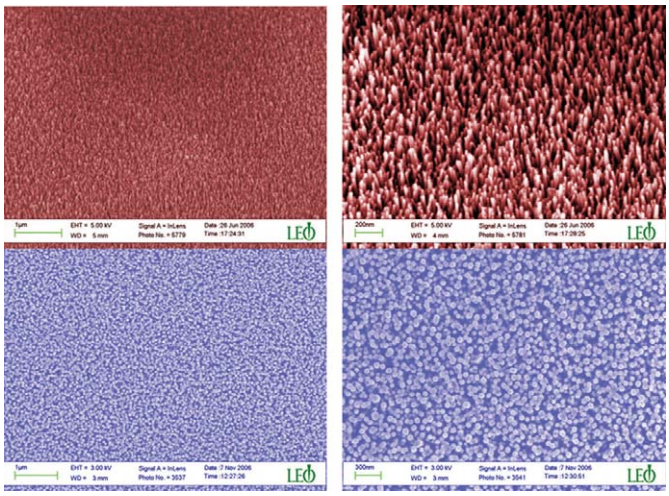

Fig. 2 SEM images of ZnO nanowire arrays grown over large surface areas on Si substrates with a ZnO-seed layer. Growth is performed in an aqueous solution of Zn nitrate hydrate and HMT at different concentrations (top: 0.025 M and bottom: 0.1 M). Substrate is tilted 45° in the top left image[42].

Table 1 summarizes some of the studies on solution growth and the resulting structures.

Electrodeposition

Electrodeposition is another method used to achieve structured nanocolumnar ZnO crystals. Various groups have obtained columns on F-doped SnO_2 (FTO) substrates between 100 nm and 300 nm in diameter and 400 nm to 900 nm in height by varying the electrodeposition parameters, such as current density, deposition time, and bath temperature[55,56]. Other groups have reported electrodeposition of thin films[57]. Findings indicate that more positive electrodeposition potentials favor high-quality film growth and additional annealing results in significant enhancement and sharpening of the excitonic emission bands[58]. The bandgap energy E_g also depends on the electrodeposition potential; with increasing potential the bandgap E_g increases. Nevertheless, the bandgap E_g depends much more strongly on film thickness, which can be explained by differences in grain size, lattice strain, and defect states[59]. Wong *et al.*[60] have shown the strong influence of the nature of the substrate surface on the nucleation of nanorods. Electropolishing of Zn foil prior to electrodeposition hinders the nucleation of nanorods. Nonelectropolished films show much narrower and denser growth of ZnO nanorods. The group conclude that a native surface oxide enhances nucleation.

Ordered porous ZnO films have been fabricated by electrodeposition on Sn-doped In-oxide (ITO) glass substrates covered with a polystyrene (PS) array template. This template is created by self-assembly of an ordered PS array from a suspension of PS spheres.

Table 1 Summary of different results and methods for aqueous solution growth.

Growth solution	Resulting morphology	Focus of investigation
Zinc nitrate, HMT	Nanorods, microtubes	On Si and conducting glass substrates[41-43]
Zinc nitrate, HMT	Nanorods, nanotubes	Influence of substrate and seed layer[44]
Zinc nitrate, HMT	Aligned nanowire arrays	Influence of seed layer[45]
Zinc-nitrate, HMT, citriate	Oriented nanocolumns, nanoplates	Control of aspect ratio: addition of citrate anions decreases aspect ratio[46]
Zinc nitrate, zinc acetate, HMT	Highly aligned nanorods	Influence of substrate and seed layer[47]
Zinc nitrate, triethanolamine, HCl (pH 5)	Ordered nanorods	Influence of substrate and counter ions in growth solution[48]
Zinc nitrate, thiourea, ammonium chloride, ammonia	Nanowires, tower-like, flower-like, tube-like	Influence of reactants, substrate pretreatment, and growth time and temperature[49]
Zinc acetate, sodium hydroxide, citric acid	Disk-like, flower-like, nanorods	Influence of pH on growth solution[50,51]
Comparison of different growth solutions	Star-like, nanorods	Influence of reaction conditions: ligand, counter-ions, pH, ionic strength, and deposition time Influence of substrate/ seed layer[52]
Zn foil, zinc sulfate, ammonium ions, sodium hydroxide	Nanobelt arrays, ordered nanowires	Influence of temperature and concentration of solutions[53,54]

Subsequently, the ZnO is electrodeposited into the pores of this array. A zinc nitrate aqueous solution is used as the electrolyte. After dissolution of the PS matrix, a stable porous ZnO film is fabricated[61]. A method to obtain ordered nanowires uses anodic alumina templates. Zn nanowires are electrodeposited with diameters of 15-90 nm into the pores of the alumina template and oxidized to ZnO in air at 300°C[62].

ZnO defect chemistry

The control of defects and associated charge carriers is of paramount importance in applications that exploit the wide range of properties of doped ZnO. However, despite the many papers on ZnO, the relationship between defect chemistry, processing, and properties has not received much attention. Despite its simple chemical formula, ZnO has a very rich defect chemistry[63]. Defect studies have been considered for more than 40 years, but now need revisiting in the context of novel applications using nanostructured materials. In the past, defect chemistry was studied in relation to ZnO properties and applications in ZnO varistors: defects significantly alter grain boundary properties and also *I-V* characteristics[64,65].

Solid surfaces contain segregated impurities, adsorbed gases that act as sources and sinks of electrons, and associated space charge regions. In nanostructured ZnO (as well as in other materials), the small length scales and large surface-to-volume ratio mean that surface defects play a stronger role in controlling properties. It is also critically important to understand defects in ZnO doped with aliovalent ions, either purposefully for achieving a certain functionality or through accidental doping during the growth process. It is important to understand the relative dominance of carriers introduced by the doping over native defects. An example is the formation of *p-n* junctions of ZnO for ultraviolet (UV) lasers. Here, achieving *p*-type ZnO with sufficient carrier concentration in a reproducible way relies on striking a careful balance between control of extrinsic doping and intrinsic defect concentration.

Before considering the defect structure of ZnO in more detail, it is important to realize that ZnO has a relatively open structure, with a hexagonal close packed lattice where Zn atoms occupy half of the tetrahedral sites. All the octahedral sites are empty. Hence, there are plenty of sites for ZnO to accommodate intrinsic (namely Zn interstitials) defects and extrinsic dopants.

The electronic energy levels of native imperfections in ZnO are illustrated in Fig. 3.

There are a number of intrinsic defects with different ionization energies. The Kröger Vink notation uses: i = interstitial site, Zn = zinc, O = oxygen, and V = vacancy. The terms indicate the atomic sites, and superscripted terms indicate charges, where a dot indicates positive charge, a prime indicates negative charge, and a cross indicates zero charge, with the charges in proportion to the number of symbols.

Fig. 3 shows that there are a number of defect states within the bandgap of ZnO. The donor defects are: $Zn_i^{\bullet\bullet}, Zn_i^{\bullet}, Zn_i^{X}, V_o^{\bullet\bullet}, V_o^{\bullet}, V_o$ and the acceptor defects are: $V_{Zn}^{''}, V_{Zn}^{'}$. The defect ionization energies vary from ~0.05-2.8 eV[66]. Zn interstitials and oxygen vacancies are known to be

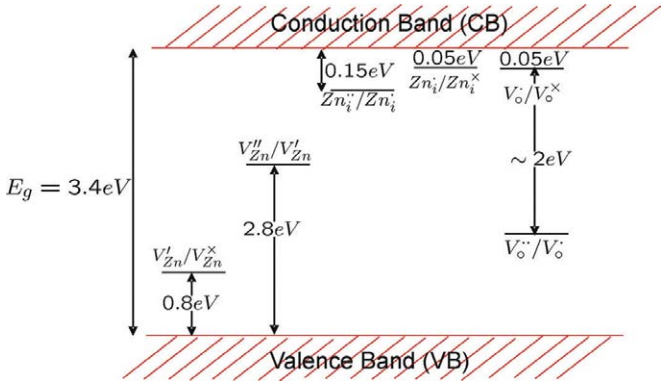

Fig. 3 Energy levels of native defects in ZnO. The donor defects are $Zn_i^{\bullet\bullet}, Zn_i^{\bullet}, Zn_i^{X}, V_o^{\bullet\bullet}, V_o^{\bullet}, V_o$ and the acceptor defects are $V_{Zn}^{''}, V_{Zn}^{'}$. (Adapted from Kröger[63])

Defect chemistry in ZnO

Zn interstitials come from the Frenkel reaction:

$$Zn_{Zn} \Leftrightarrow Zn_i^X + V_{Zn}^X$$

Further ionization reactions and equilibrium constants are[66]:

$$Zn_i^X \Leftrightarrow Zn_i^\bullet + e' \qquad K = 2N_c \exp(-0.05/kT)$$
$$Zn_i^\bullet \Leftrightarrow Zn_i^{\bullet\bullet} + e' \qquad K = 1/2N_c \exp(-0.15/kT)$$

The oxygen vacancies arise from the Schottky reaction:

$$0 \Leftrightarrow V_{Zn}^\times + V_O^\times$$

Further ionization reactions and equilibrium constants are:

$$V_O^X \Leftrightarrow V_O^\bullet + e' \qquad K = 2N_C \exp(-0.05/kT)$$
$$V_O^\bullet \Leftrightarrow V_O^{\bullet\bullet} + e' \qquad K = 1/2N_C \exp(-2.0/kT)$$

$$V_{Zn}^\times \Leftrightarrow V_{Zn}' + h^\bullet \qquad K = 2N_V \exp(-0.8/kT)$$
$$V_{Zn}' \Leftrightarrow V_{Zn}'' + h^\bullet \qquad K = 1/2N_V \exp(-2.8/kT)$$

the predominant ionic defect types. However, which defect dominates in native, undoped ZnO is still a matter of great controversy[67]. As shown in the text box, both defects donate two electrons and so it is difficult to distinguish one from the other using electrical measurements.

Because of the different ionization energies, the relative concentrations of the various defects depend strongly on temperature. However, the partial pressure of oxygen and zinc, pO_2 and pZn, respectively, are also very important. Hence, under very reducing conditions and at high temperatures, oxygen vacancies may predominate, depending on the relative pO_2/pZn ratio. Zn interstitials are the predominant defects under Zn vapor rich environments. Zn evaporates readily in a Zn-poor environment, even at temperatures as low as 500°C and after annealing for only a matter of hours[68]. In order to maintain a Zn interstitial concentration, annealing is required in the presence of Zn vapor followed by rapid quenching[69]. Solubility from saturated Zn vapor is calculated[68] to be n = 3.4 x10^{20} exp(-0.65e/kT) atoms/cm^3.

Even when the oxygen vacancy concentration is of a similar level to the Zn interstitial concentration, the ionization energy of the doubly charged oxygen vacancy is still much higher than for a Zn interstitial. Hence, the conductivity arising from the associated electronic carriers is lower than if the vacancies were easily ionized. It is also important to note that the kinetics of oxidation/de-oxidation are relatively slow at <1300°C and, hence, unless very reducing conditions are used, the oxygen vacancy concentration is not easily changed at <1000°C.

In regard to the defects in different pZn and pO_2 regimes, Brouwer diagrams are used that plot log[defect or carrier concentration] versus log pO_2 or log pZn. These diagrams are very useful to show which defects dominate under different experimental conditions. A Brouwer diagram for ZnO showing the variation of different defects with log pO_2 is given in Fig. 4[69]. It shows that charged oxygen vacancies dominate in the low pO_2 regime. However, other researchers maintain that Zn interstitials dominate in the low pO_2 regime[70]. This difference is likely to be a result of the influence of pZn, i.e. at low pO_2 and high pZn, it is probable that Zn interstitials dominate, whereas at low pO_2 and low pZn, it is probable that oxygen vacancies dominate.

There is wide agreement that there is a switch to Zn vacancy domination at higher pO_2 (the transition region depends on temperature: at 1300°C, it is at above pO_2 = 1 atm). In terms of pZn, there is a switch from Zn vacancy domination at low pZn to Zn interstitials at higher pZn[67]. At 1000°C, the transition occurs at around pZn ~10^{-10} atm[67]. The power dependencies of the slopes in Fig. 4 (-1/6 and ±1/2) arise from the relevant defect equilibria. For further information on this subject, the reader is referred to[71]. Carrier concentrations can vary by several orders of magnitude across the Brouwer diagram[72].

Impurities and deliberate doping with aliovalent (differently charged) ions have marked effects on the defect equilibria and this is very important to consider when nanostructures are grown in the presence of other atomic species. Carriers are introduced depending on whether the ions have a lower valence (e.g. Li^{1+} introduces holes) or higher valence (e.g. Al^{3+} introduces electrons) than the Zn. There is no pO_2 or pZn dependence on the carrier concentration from such substitutions, but very small atomic concentrations (>10^{16} cm^{-3}) can outweigh the intrinsic defects in the middle pO_2 or pZn regions, leading to a plateau in carrier concentration over several decades of partial pressure.

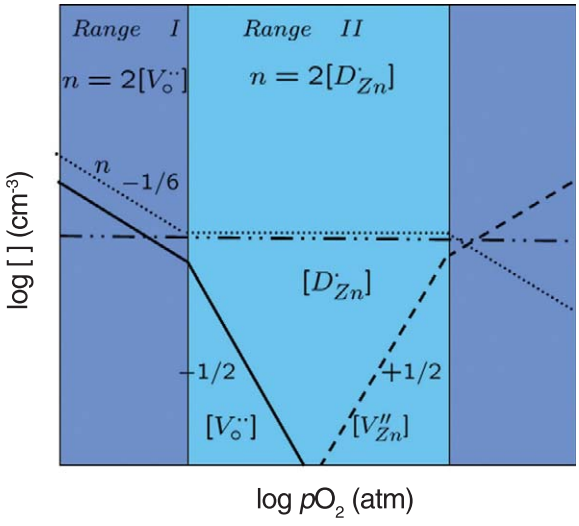

Fig. 4 Schematic Brouwer diagram showing a transition from intrinsic defect control by $V_0^{\cdot\cdot}$ (range I) to extrinsic defect control from an unknown charged donor impurity $D^{\cdot}_{Zn}$, (e.g. an ion of 3+ valence) (range II). [ ] on the left-hand axis indicates concentration of defects. The far right-hand region (unlabeled) corresponds to V'_{Zn} control. (Adapted from[69].)

Table 2 Summary of different doped ZnO films as transparent conductors.

Dopant	Transmittance in visible range	Lowest resistivity	Methods
Al	~90%	~10^{-4} Ωcm	Pulsed laser deposition (PLD)[82-85]
			Radio-frequency (RF) magnetron sputtering[86]
			Solution processed[87,88]
Ga	~85%	~10^{-3} Ωcm	PLD[89]
			Solution processed[90]
In	~80%	~20 Ωcm	Solution processed[91]
N	~80%	~10^{-2} Ωcm	Plasma-assisted molecular beam epitaxy[92]
			RF magnetron sputtering[93]
			Solution processed[13,94,95]

Examples of doped ZnO

Selective element doping offers a method to adjust the electrical, optical, and magnetic properties of ZnO nanowires, which is important for applications. Many types of dopants have been introduced (e.g. Sn[73], As[74], S[75], Cd[76], FeCo[77], In[78], Cu[79], Mn[80], Al[81] etc.). Doped ZnO films are promising candidates as conductors with high transparency in the visible light range and high conductivity. Even though the standard transparent conductors in industry are ITO and FTO, there is huge interest in finding more stable and cheaper alternatives. Typical dopants that have been employed to increase the conductivity of ZnO are group III (B, Al, In, Ga) and group IV (Pb, Sn) elements of the periodic table. Table 2 summarizes some doped films, their transmittance in the visible range, and lowest resistivity values.

Applications

Sensors

ZnO nanostructures have been widely used for sensing applications because of their high sensitivity to the chemical environment. Nanostructures have the advantage of a high surface area, and electronic processes are strongly influenced by surface processes. ZnO nanowires have demonstrated high sensitivity even at room temperature, whereas thin-film gas sensors often need to be operated at elevated temperatures.

The sensing process is governed by oxygen vacancies on the surface that influence the electronic properties of ZnO. Upon oxidation, via adsorption of molecules such as NO_2 at vacancy sites that accept electrons, electrons are withdrawn and effectively depleted from the conduction band, leading to a reduction of conductivity. On the other hand, reducing molecules such as H_2 can react with surface-adsorbed oxygen, leaving behind an electron and a higher conductivity. The challenge is to sense certain gases selectively.

A ZnO nanorod H_2 sensor has been developed[96]. The sensitivity of this sensor was improved by sputter deposition of Pd clusters on the ZnO rod surface. The addition of Pd appears to be effective in the catalytic dissociation of H_2 into atomic hydrogen, increasing the sensitivity of the sensor device. The sensor detects hydrogen concentrations down to 10 ppm in N_2 at room temperature, whereas there is no response to O_2. By exposing the sensor to air or O_2, the conductance recovers to 95% after 20 s. The same group have also shown H_2 sensitivity for Pt-coated ZnO nanorods[97].

A different group used a thick film of ZnO nanoparticles for H_2 sensing[98]. A sensitivity of 10-1000 ppm H_2 was achieved for a Pt-impregnated, 3% Co-doped ZnO nanoparticle film at a working temperature of 125°C or lower. O_2, NO_2, and NH_3 oxidizing sensors in a field-effect transistor geometry of single nanowires have also been demonstrated[99,100]. The oxygen sensitivity is higher for smaller diameter nanowires and can be modulated by the gate voltage. Desorption of adsorbed NO_2 molecules is observed when a large negative gate voltage is applied. This can be used as a method to refresh the sensor to its original level. An ethanol sensor with good sensitivity and fast response at 300°C has been demonstrated using Pt interdigitating electrodes[101].

Tetrapod-films prepared in a flow of humidified Ar show excellent performance in sensing ethanol with a short response time[102]. A photocurrent gas sensor made of Ru-sensitized ZnO nanoparticles has been shown to be highly influenced by the gas molecules adsorbed on the surface[103]. A CO molecule increases the number of electrons on the surface of ZnO and, therefore, leads to an increase in photoconductivity. On the contrary, O_2 can capture electrons directly on the surface and lower the concentration of charge carriers in the ZnO conduction band and, therefore, the photoconductivity. A glucose sensor based on ZnO nanorods has also been reported[104]. The negatively charged glucose oxidase (GOx) enzyme is immobilized on positively charged ZnO through electrostatic forces. At an applied potential of +0.8 V versus a Ag/AgCl reference electrode, the glucose biosensor shows a linear response from 0.01-3.45 mM and experiment limit of detection of 0.01 mM. The response time was less than 5 s.

Light-emitting diodes and lasing

Bao *et al.*[105] have constructed a single nanowire light-emitting diode. They disperse ZnO nanowires on a Si substrate and then a poly(methyl methacrylate), or PMMA, thin film is spin-coated onto the substrate. The wire is imaged in a focus ion beam (FIB) system and a pattern for e-beam exposure of the PMMA is defined. The unexposed and partially exposed PMMA is removed and then a metallic contact is deposited onto the top surface of a single nanowire. In this way, the researchers are able to measure the current-voltage characteristics, photoluminescence, and electroluminescence of a single nanowire (Fig. 5).

A ZnO homojunction light-emitting diode (LED) has been fabricated on a single-crystal GaAs substrate by ultrasonic-assisted spray

pyrolysis[106]. The diode consists of a N-In co-doped *p*-type ZnO and a *n*-type ZnO film. The homojunction LED shows a threshold voltage of ~4 V under forward bias. A hybrid light-emitting *p-n* junction diode has been produced using ZnO nanorods as the *n*-type material and the hole-conducting polymer poly-2,4-ethylene dioxythiophene poly(styrenesulfonate), or (PEDOT/PSS), as the *p*-type material. PS was used to isolate neighboring nanorods. In the electroluminescence spectrum, ZnO band edge emission at 383 nm is observed, as well as peaks at 430 nm, 640 nm, and 748 nm. The threshold bias for UV light emission is 3 V[68]. The same structure has been used by Könenkamp *et al.*[107], giving similar results.

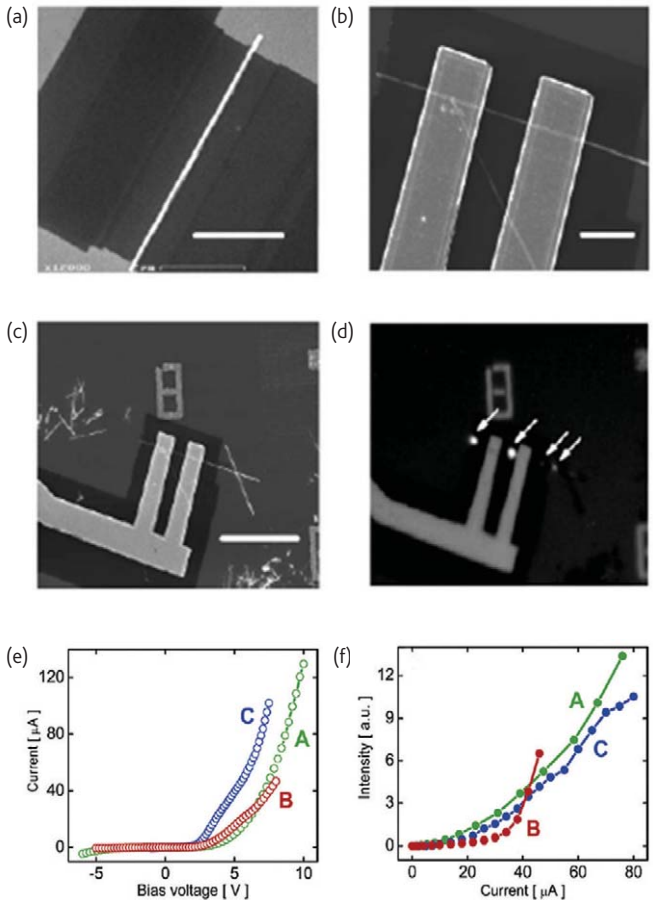

Fig. 5 (a) SEM image of a finished pattern on a ZnO nanowire before metal deposition. Light gray, p-Si substrate; dark gray, crosslinked PMMA; white, ZnO nanowire. Scale bar is 2 μm. (b) SEM image of a typical finished device. The top Ti/Au metallic electrodes (~50 nm Ti and ~120 nm Au) contact the wire twice, leaving three open sections for light emission. The exposed top nanowire surface is visible. Note that the nanowire placed diagonally across the metallic pads is electrically insulated from the latter by a thin layer of crosslinked PMMA. The scale bar is 2 μm. (c) Lower magnification SEM image of (b). The less dark area is the p-Si substrate, and darkest one is crosslinked PMMA. A stray ZnO nanowire intercepts the device on the right-hand side. Scale bar is 10 μm. (d) Grayscale optical image of the device when 7 V is applied to the substrate electrode with respect to the metallic contact. The light emission comes from four spots, indicated by the arrows. (e) Current versus voltage of three finished devices at room temperature and ambient air. The solid lines are a guide to the eye. Device A corresponds to the device shown in (b)-(d). Positive voltage corresponds to the voltage of the p-Si substrate with respect to the top metallic contact. (f) Light intensity versus current for forward bias. Light is collected directly above the sample using a microscope objective with 50x magnification. (Reprinted with permission from[105]. © 2006 American Chemical Society.)

Lasing in ZnO nanowire arrays grown by a variety of methods has been observed by different groups. Huang *et al.*[108] have used nanowires grown by CVD on sapphire and shown a threshold of 40 KW/cm^2 under optical excitation. For the first time, lasing of solution-grown ZnO nanorod arrays grown on F-doped SnO_2 glass substrates has been observed[109]. Stimulated emission has also been observed for solution-grown ZnO on Si[110]. The observed UV-lasing efficiency is similar to that reported for nanowire arrays grown on Al_2O_3 substrates in a high-temperature process. A dielectrophoretic effect has been used to trap nanowires in a microelectrode gap. These devices can then be used as UV detectors[111] and show a remarkably high sensitivity to UV light down to 10 nW/cm^2.

Cantilevers

Lee *et al.*[112] have proposed the use of well-aligned single-crystalline nanowires for use as sharp atomic force microscopy (AFM) tips. They predict that ZnO nanowires are structurally compatible with AFM cantilevers under typical operating conditions, and are promising candidates for high-aspect-ratio probes for AFM. Huang *et al.*[113] have characterized the mechanical resonances of a single nanowire using an alternating electric field. They have monitored the flexural mode of the nanowire *in situ* in a transmission electron microscope (TEM). With an elastic bending modulus of ~58 GPa and a damping time constant of ~14 ms for the resonance in vacuum, the authors conclude that a single ZnO nanowire can be used as a nanoresonator and a nanoscale cantilever.

Solar cells

Recently, ZnO has been used in dye-sensitized solar cells as an electrode material[114-117]. Investigations of nanoporous dye-sensitized ZnO films have shown that ultrafast electron injection from the dye into the conduction band of the ZnO particles takes place[118-121], comparable to the timescale of electron injection into TiO_2 layers, which has been the subject of investigation for a long time[122]. Semiconductors should have a wide bandgap, high charge carrier mobility, and films fabricated from the material need to deliver a high surface area for efficient dye-sensitization and light harvesting, which can only be achieved by a nanostructured film. Therefore, ZnO seems to be a promising material for this type of solar cell and has the advantage over other metal oxides of easy synthesis of controlled nanostructures. Dye-sensitized solar cells usually have an electrolyte (redox system) to regenerate the dye by electron donation to its ground state after excitation.

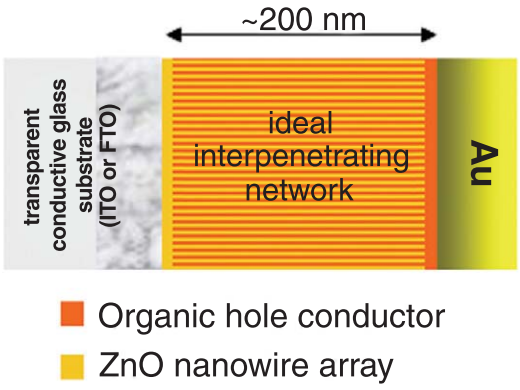

Fig. 6 Schematic of a hybrid solar cell with an ideal interpenetrating network consisting of highly aligned and ordered ZnO nanowires and an organic hole transporter material.

The use of a solid organic hole-transporter material to replace the liquid electrolyte has been investigated more recently[123]. In this case, an organic hole-transporting material is infiltrated into the nanoporous structure. The challenge for these solar cells is filling the pores of the nanoporous layer[124,125]. Only very few organic hole-transporter materials are able to fill the nanoporous TiO_2 layer. In general, polymers seem to block the pores and do not lead to efficient pore filling. This has led to the use of nanowire arrays as promising candidates for hybrid solar cell applications. The possibility of using a broad range of organic hole-transporter materials makes this approach very attractive, even though the surface area of a nanowire array is much smaller than that of a nanoporous layer of the same thickness. Therefore, in addition to the dye being a sensitizer, it also has to serve as a light-absorbing material and contribute to charge generation. Compared to fully organic solar cells, nanostructured hybrid solar cells have the advantage that the morphology of the film can be controlled by growth of the ZnO structure. The ZnO serves as an electrode material, as well as being a template for nanoscale phase separation. Devices have a sandwich-like structure (Fig. 6). The ZnO nanowire arrays are grown onto conducting glass substrates and filled with the organic material. A top electrode metal is then evaporated.

Recently, poly(3-hexylthiophene) (P3HT) has been used as a hole transporter in combination with ZnO nanostructures. These devices have an efficiency of ~0.5% under standard solar conditions (AM 1.5, 100 mW/cm^2)[126] and show a current density of J_{SC} = 2.2 mA/cm^2, an open circuit voltage of V_{OC} = 440 mV, and a fill factor of 56%. This cell performance can be significantly improved to J_{SC} = 10.0 mA/cm^2, V_{OC} = 475 mV, and a fill factor of 43% leading to an efficiency of 2% by using a blend of P3HT and (6,6)-phenyl C_{61} butyric acid methyl ester (PCBM). The low open circuit voltage in hybrid solar cells using ZnO as the electrode material is not yet fully understood. Certainly, more investigation is necessary to find the leakage and then higher cell efficiencies can be expected. Ravirajan *et al.*[127] have systematically investigated the influence of the ZnO structure on the device performance. They compared flat ZnO layers, ZnO nanoporous layers, and vertically aligned nanowires. The charge recombination time in the vertically aligned ZnO nanorods is remarkably slow and gives a half-life of several milliseconds, over two orders of magnitude slower than that for nanoparticles, which should be advantageous for solar cell applications. In a solar cell structure with P3HT as a hole transporter and sensitized with an amphiphilic Ru dye, the performance is still four times higher in the aligned nanorod structure than in the nanoparticle structure. These investigations suggest that nanowire structures will further enhance the performance of hybrid solar cells in the future.

Conclusion

The unique properties of ZnO and the ease of ZnO nanostructure fabrication make this material extremely interesting for applications. In recent years, the number of applications of ZnO nanostructures has risen dramatically and this can be expected to be just the beginning. The examples shown in this review give only a brief indication of the possible applications. The versatility of properties and formation of nanostructures makes it likely that new ideas will also come up in the future, leading to new device applications, some of which are already under intense research investigation. mt

Acknowledgments

The authors acknowledge funding from the European Commission (Marie Curie Excellence Grant 'NanoFen', MEXT-CT-2004-014156). LSM also thanks the Royal Society for funding.

REFERENCES

1. Pearton, S. J., *et al.*, *Prog. Mater. Sci.* (2005) **50**, 293
2. Özgür, Ü., *et al.*, *Appl. Phys. Rev.* (2005) **98**, 041301
3. Norton, D. P., *et al.*, *Materials Today* (2004) **7** (6), 34
4. Heo, Y. W., *et al.*, *Mater. Sci. Eng. R* (2004) **47**, 1
5. Pearton, S. J., *et al.*, *Superlattices Microstruct.* (2003) **34**, 3
6. Yi, G.-C., *et al.*, *Semicond. Sci. Technol.* (2005) **20**, S22
7. Wang, Z. L., *Materials Today* (2004) **7** (6), 26
8. Look, D. C., *Mater. Sci. Eng. B* (2001) **80**, 383
9. Chambers, S. A., *et al.*, *Materials Today* (2006) **9** (11), 28
10. Iwata, K., *et al.*, *Thin Solid Films* (2004) **451-452**, 219
11. Ip, K., *et al.*, *J. Cryst. Growth* (2006) **287**, 149
12. Look, D. C., *Semicond. Sci. Technol.* (2005) **20**, S55
13. Coa, Y., *et al.*, *Appl. Phys. Lett.* (2006) **88**, 251116
14. Wagner, R. S., and Ellis, W. C., *Appl. Phys. Lett.* (1964) **4**, 89
15. Yang, P., *et al.*, *Adv. Funct. Mater.* (2002) **12**, 323
16. Wang, X. D., *et al.*, *Nano Lett.* (2004) **4**, 423
17. Wang, X. D., *et al.*, *J. Am. Chem. Soc.* (2005) **127**, 7920
18. Ramgir, N. S., *et al.*, *J. Phys. Chem. B* (2006) **110**, 18236

19. Song, J. H., *et al.*, *J. Phys. Chem. B* (2005) **109**, 9869
20. Park, J.-H., and Park, J.-G., *Curr. Appl. Phys.* (2006) **6**, 1020
21. Huang, M. H., *et al.*, *Adv. Mater.* (2001) **13**, 113
22. Greyson, E. C., *et al.*, *Adv. Mater.* (2004) **16**, 1348
23. Meng, X., *et al.*, *Solid State Commun.* (2005) **135**, 411
24. Jie, J., *et al.*, *Appl. Phys. Lett.* (2005) **86**, 031909
25. Ng, H. T., *et al.*, *Appl. Phys. Lett.* (2003) **82**, 2023
26. Hu, P., *et al.*, *Chem. Commun.* (2003), 1304
27. Pan, Z. W., *et al.*, *Nano Lett.* (2005) **5**, 723
28. Zhang, J., *et al.*, *J. Cryst. Growth* (2005) **280**, 509
29. Lee, W., *et al.*, *Nanotechnology* (2004) **15**, 254
30. Wu, J.-J., and Liu, S.-C., *Adv. Mater.* (2002) **14**, 215
31. Tak, Y., *et al.*, *J. Vac. Sci. Technol. B* (2006) **24**, 2047
32. Pan, Z. W., *et al.*, *Science* (2001) **291**, 1947
33. Gao, P. X., *et al.*, *Science* (2005) **309**, 1700
34. Gao, P. X., and Wang, Z. L., *Small* (2005) **1**, 945
35. Gao, P. X., and Wang, Z. L., *J. Appl. Phys.* (2005) **97**, 044304
36. Kong, X. Y., and Wang, Z. L., *Nano Lett.* (2003) **3**, 1625
37. Hughes, W. L., and Wang, Z. L., *J. Am. Chem. Soc.* (2004) **126**, 6703
38. Kong, X. Y., *et al.*, *Science* (2004) **303**, 1348
39. Wang, Z. L., *Annu. Rev. Phys. Chem.* (2004) **55**, 159
40. Andrés Vergés, M., *et al.*, *J. Chem. Soc., Faraday Trans.* (1990) **86**, 959
41. Vayssieres, L., *et al.*, *J. Phys. Chem. B* (2001) **105**, 3350
42. Schmidt-Mende, L., *et al.*, (2007) unpublished
43. Vayssieres, L., *Adv. Mater.* (2003) **15**, 464
44. Sun, Y., *et al.*, *J. Phys. Chem. B* (2006) **110**, 15186
45. Greene, L. E., *et al.*, *Nano Lett.* (2005) **5**, 1231
46. Tian, Z. R., *et al.*, *Nat. Mater.* (2003) **2**, 821
47. Chen, Z., and Gao, L., *J. Cryst. Growth* (2006) **293**, 522
48. Boyle, D. S., *et al.*, *Chem. Commun.* (2002), 80
49. Wang, Z., *et al.*, *Langmuir* (2004) **20**, 3441
50. Zhang, H., *et al.*, *Cryst. Growth Des.* (2005) **5**, 547
51. Zhang, H., *et al.*, *Mater. Lett.* (2005) **59**, 1696
52. Govender, K., *et al.*, *J. Mater. Chem.* (2004) **14**, 2575
53. Xu, F., *et al.*, *J. Non-Cryst. Solids* (2006) **352**, 2569
54. Lu, C., *et al.*, *Chem. Commun.* (2006) 3551
55. Cembrero, J., *et al.*, *Thin Solid Films* (2004) **451-452**, 198
56. Marí, B., *et al.*, *Microelectron. J.* (2004) **35**, 79
57. Fahoume, M., *et al.*, *Sol. Energy Mater. Sol. Cells* (2006) **90**, 1437
58. Wang, Q., *et al.*, *Thin Solid Films* (2005) **492**, 61
59. Marotti, R. E., *et al.*, *Sol. Energy Mater. Sol. Cells* (2004) **82**, 85
60. Wong, M. H., *et al.*, *Nanotechnology* (2003) **14**, 968
61. Liu, Z., *et al.*, *Semicond. Sci. Technol.* (2006) **21**, 60
62. Li, Y., *et al.*, *Appl. Phys. Lett.* (2000) **76**, 2011
63. Kröger, F. A., *The Chemistry of Imperfect Crystals*. 2nd Edition, North Holland, Amsterdam (1974), 73
64. Mahan, G. D., *J. Appl. Phys.* (1983) **54**, 3825
65. Gupta, T. K., *J. Am. Ceram. Soc.* (1990) **73**, 1817
66. Han, J., *et al.*, *J. Eur. Ceram. Soc.* (2002) **22**, 49
67. Hagemark, K. I., *J. Solid State Chem.* (1976) **16**, 293
68. Thomas, D. G., *J. Phys. Chem. Solids* (1957) **3**, 229
69. Tomlins, G. W., *et al.*, *J. Appl. Phys.* (2000) **87**, 117
70. Wuensch, B. J., and Tuller, H. J., *J. Phys. Chem. Solids* (1994) **55**, 975
71. Kingery, W. D., *et al.*, *Introduction to Ceramics*. 2nd Edition, John Wiley and Sons, New York, (1976)
72. Hagemark, K. I., and Chacka, L. C., *J. Solid State Chem.* (1975) **15**, 261
73. Li, Y. S., *et al.*, *J. Phys. D: Appl. Phys.* (2004) **37**, 2274
74. Lee, W., *et al.*, *Appl. Phys. Lett.* (2004) **85**, 6167
75. Shen, G., *et al.*, *J. Phys. Chem. B* (2005) **109**, 5491
76. Li, Q. H., *et al.*, *Appl. Phys. Lett.* (2005) **86**, 263101
77. Liu, L. Q., *et al.*, *Appl. Phys. Lett.* (2006) **88**, 63104
78. Xu, L., *et al.*, *J. Phys. Chem. B* (2006) **110**, 6637
79. Xu, C. X., *et al.*, *Nanotechnology* (2004) **15**, 856
80. Liu, J. J., *et al.*, *Appl. Phys. Lett.* (2005) **87**, 172505
81. Wang, R.-C., *et al.*, *Appl. Phys. Lett.* (2006) **88**, 23111
82. Agura, H., *et al.*, *Thin Solid Films* (2003) **445**, 263
83. Suzuki, A., *et al.*, *Jpn. J. Appl. Phys.* (1996) **35**, L56
84. Holmelund, E., *et al.*, *Appl. Phys. A* (2004) **79**, 1137
85. Tanaka, H., *et al.*, *J. Vac. Sci. Technol. A* (2004) **22**, 1757
86. Jeong, W. J., *et al.*, *Thin Solid Films* (2006) **506-507**, 180
87. Valle, G. G., *et al.*, *J. Eur. Ceram. Soc.* (2004) **24**, 1009
88. Ma, G., *et al.*, *Surf. Rev. Lett.* (2006) **13**, 13
89. Henley, S. J., *et al.*, *Surf. Coat. Technol.* (2004) **177-178**, 271
90. Gomez, H., *et al.*, *Sol. Energy Mater. Sol. Cells* (2005) **87**, 107
91. Kumar, P. M. R., *et al.*, *Semicond. Sci. Technol.* (2005) **20**, 120
92. Jiao, S. J., *et al.*, *Appl. Phys. Lett.* (2006) **88**, 031911
93. Lin, C.-C., *et al.*, *Appl. Phys. Lett.* (2004) **84**, 5040
94. Zhao, J.-L., *et al.*, *J. Cryst. Growth* (2005) **280**, 495
95. Zhang, C. Y., *et al.*, *Chem. Phys. Lett.* (2006) **420**, 448
96. Wang, H. T., *et al.*, *Appl. Phys. Lett.* (2005) **86**, 243503
97. Tien, L. C., *et al.*, *Appl. Phys. Lett.* (2005) **87**, 222106
98. Rout, C. S., *et al.*, *Solid State Commun.* (2006) **138**, 136
99. Fan, Z., *et al.*, *Appl. Phys. Lett.* (2004) **85**, 5923
100. Fan, Z., and Lu, J. G., *Appl. Phys. Lett.* (2005) **86**, 123510
101. Wan, Q., *et al.*, *Appl. Phys. Lett.* (2004) **84**, 3654
102. Xiangfeng, C., *et al.*, *Chem. Phys. Lett.* (2005) **401**, 426
103. Yang, M., *et al.*, *Sens. Actuators B* (2006) **117**, 80
104. Wei, A., *et al.*, *Appl. Phys. Lett.* (2006) **89**, 123902
105. Bao, J., *et al.*, *Nano Lett.* (2006) **6**, 1719
106. Du, G. T., *et al.*, *Appl. Phys. Lett.* (2006) **89**, 052113
107. Könenkamp, R., *et al.*, *Nano Lett.* (2005) **5**, 2005
108. Huang, M. H., *et al.*, *Science* (2001) **292**, 1897
109. Govender, K., *et al.*, *Adv. Mater.* (2002) **14**, 1221
110. Choy, J.-H., *et al.*, *Adv. Mater.* (2003) **15**, 1911
111. Suehiro, J., *et al.*, *Nanotechnology* (2006) **17**, 2567
112. Lee, W., *et al.*, *Acta Mater.* (2004) **52**, 3949
113. Huang, Y., *et al.*, *J. Phys.: Condens. Matter* (2006) **18**, L179
114. Bedja, I., *et al.*, *Langmuir* (1997) **13**, 2398
115. Keis, K., *et al.*, *J. Photochem. Photobiol. A* (2002) **148**, 57
116. Keis, K., *et al.*, *Sol. Energy Mater. Sol. Cells* (2002) **73**, 51
117. Keis, K., *et al.*, *J. Electrochem. Soc.* (2001) **148**, A149
118. Katoh, R., *et al.*, *J. Photochem. Photobiol. A* (2004) **166**, 69
119. Katoh, R., *et al.*, *J. Phys. Chem. B* (2004) **108**, 4818
120. Furube, A., *et al.*, *J. Phys. Chem. B* (2003) **107**, 4162
121. Horiuchi, T., *et al.*, *J. Phys. Chem. B* (2003) **107**, 2570
122. O'Regan, B., and Grätzel, M., *Nature* (1991) **353**, 737
123. Bach, U., *et al.*, *Nature* (1998) **395**, 583
124. Schmidt-Mende, L., and Grätzel, M., *Thin Solid Films* (2006) **500**, 296
125. Kroeze, J. E., *et al.*, *Adv. Funct. Mater.* (2006) **16**, 1832
126. Olson, D. C., *et al.*, *Thin Solid Films* (2006) **496**, 26
127. Ravirajan, P., *et al.*, *J. Phys. Chem. B* (2006) **110**, 7635